JACS
JOURNAL OF THE AMERICAN CHEMICAL SOCIETY
Communication
pubs.acs.org/JACS

Enhanced Cycling Stability of Hybrid Li–Air Batteries Enabled by Ordered Pd_3Fe Intermetallic Electrocatalyst

Zhiming Cui,[#] Longjun Li,[#] Arumugam Manthiram, and John B. Goodenough*

Materials Science and Engineering Program & Texas Materials Institute, The University of Texas at Austin, Austin, Texas 78712, United States

Supporting Information

ABSTRACT: We report an ordered Pd_3Fe intermetallic catalyst that exhibits significantly enhanced activity and durability for the oxygen reduction reaction under alkaline conditions. Ordered Pd_3Fe enables a hybrid Li–air battery to exhibit the best reported full-cell cycling performance (220 cycles, 880 h).

Lithium–air batteries have been investigated as good candidates among the rechargeable batteries for use in electric vehicles owing to their higher energy density compared to that of Li-ion batteries. For the widely investigated aprotic Li–air battery, the theoretical energy density reaches as high as 3504 Wh kg^{-1}.[1] However, the practical energy density of aprotic Li–air batteries is limited by the deposition of the insoluble discharge products (Li_2O_2) clogging the air electrodes, the decomposition of organic electrolytes, and the need for excess packaging to keep the battery in a dry oxygen environment.[2] To overcome these problems, a hybrid system has been developed, composed of a nonaqueous electrolyte in the anode side (oxidation of Li to Li^+) and an aqueous electrolyte in the cathode side (reduction of oxygen in the presence of Li^+), separated by a solid lithium-ion-conducting electrolyte. However, the cycle life of such hybrid systems is limited. The problem lies mainly in the sluggish kinetics of the oxygen reduction reaction (ORR) and poor durability of the cathode catalyst, which actually is also the major limiting factor for other energy conversion and storage technologies, such as fuel cells and metal–air batteries. Therefore, it is desirable to develop highly active and stable electrocatalysts for the ORR in aqueous media.

Pt and Pt-based alloys remain the most efficient ORR catalysts, but their high cost and scarcity have made them increasingly unattractive for such applications.[3] Low-cost alternatives such as N-doped carbon materials,[4,5] metal oxides,[6,7] and perovskites[8] have been explored but are still far from meeting the requirement of combined high catalytic activity and durability. As a potential replacement for the Pt catalyst, Pd has attracted considerable attention because of its high catalytic activity, relatively lower cost, and higher abundance (~50 times more abundant than Pt).[9,10] Recent studies have shown that supported Pd and Pd-based alloys exhibit ORR activity comparable to that of Pt/C in alkaline media. However, most reports have focused mainly on the disordered Pd-based alloy catalysts, which have varying surface composition and thus randomly distributed active sites. Structurally ordered Pd-based intermetallic compounds have never been reported as ORR catalysts. In an ordered intermetallic phase, every crystallographic site is occupied by only one type of atom; therefore, an ordered phase can provide predictable control over structural, geometric, and electronic effects. Further, as the order in intermetallic phases arises from the high enthalpy of mixing, a high chemical and structural stability can be expected. Apparently, ordered intermetallic catalysts possess different catalytic properties in comparison to their disordered alloys. Recent reports on Pt-based alloys suggest that ordered phases show better performance compared to their disordered alloys for both the anodic and cathodic reactions in fuel cells.[11,12] The discovery of ordered Pt-based catalysts inspired us to investigate Pd-based intermetallic catalysts. Herein we report an ordered Pd_3Fe intermetallic catalyst that exhibits significantly enhanced activity and durability for the ORR relative to disordered Pd_3Fe/C, Pd/C, and Pt/C. An ordered Pd_3Fe-enabled hybrid Li–air battery exhibits the best reported cycling performance so far: over 200 cycles (more than 800 h) with only 0.08 V increase in round-trip overpotential based on discharge and charge end voltages.

To form the ordered intermetallic phases, thermal annealing is generally necessary; this often results in significant agglomeration and particle-size growth.[11] It is critical to choose a suitable synthetic route for controlling both the ordering and particle size of the ordered intermetallic catalysts. Recently, Chen et al. reported a KCl matrix method for the synthesis of ordered Pt-based intermetallic catalysts with controlled particle size.[13] Here, we modify that method and extend it to the synthesis of ordered Pd_3Fe intermetallic catalysts. Potassium triethylborohydride (KEt_3BH) was selected as a reducing agent because it not only has fast reducing kinetics but also produces an insoluble byproduct, KCl. The KCl matrix can encapsulate Pd_3Fe particles, preventing their agglomeration during annealing. The experimental details and a schematic preparation procedure (Figure S1) are presented in the Supporting Information (SI). We also explore the factors that control the ordering behavior of Pd_3Fe under various annealing conditions. The sample annealed at 600 °C is denoted as ordered Pd_3Fe/C, and the sample annealed at 400 °C is denoted as disordered Pd_3Fe/C.

Figure 1 shows the XRD pattern for ordered Pd_3Fe/C and disordered Pd_3Fe/C along with that of Pd/C catalyst for a comparison. The XRD pattern of Pd/C shows five peaks at

Received: April 14, 2015
Published: May 28, 2015

DOI: 10.1021/jacs.5b03865
J. Am. Chem. Soc. 2015, 137, 7278–7281

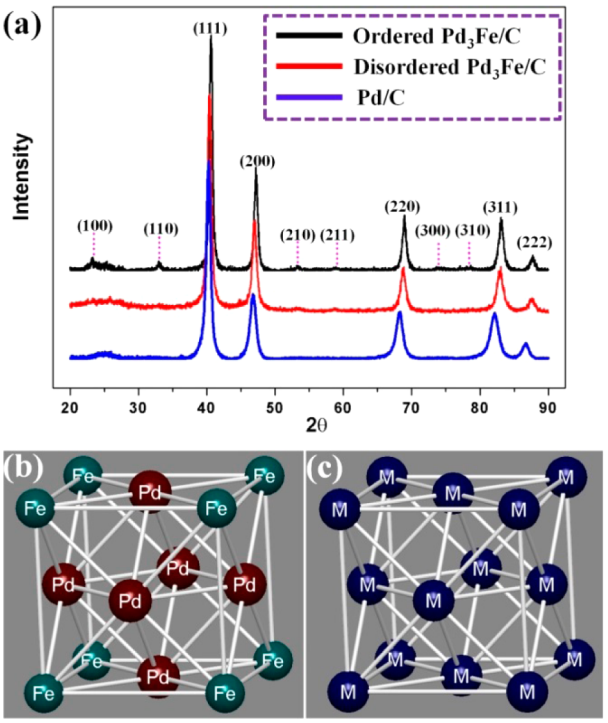

Figure 1. (a) XRD patterns of ordered Pd_3Fe/C, disordered Pd_3Fe/C, and Pd/C. Drop lines correspond to Pd_3Fe (PDF Card 65-7280). (b) Crystal structure of ordered Pd_3Fe. (c) Crystal structure of disordered Pd_3Fe.

40.1°, 46.7°, 68.1°, 82.1°, and 86.2°, which are consistent with the (111), (200), (220), (311), and (222) reflections of pure Pd (face-centered-cubic (fcc)-type structure: $Fm\bar{3}m$; a = 3.890 Å). For disordered Pd_3Fe/C, its XRD pattern clearly shows the five main characteristic peaks of the fcc crystalline Pd, demonstrating it to be a disordered alloy structure (solid solution). The peaks of disordered Pd_3Fe/C shift slightly to higher angles relative to Pd/C, which is attributed to the decrease in the lattice constant. In the case of ordered Pd_3Fe/C, there are six additional peaks appearing at 23.1°, 32.9°, 53.2°, 58.7°, 73.8°, and 78.5° compared to Pd/C; they are assigned to the (100), (110), (210), (211), (300), and (310) ordering reflections of Pd_3Fe in the Cu_3Au structure type ($Pm\bar{3}m$, a = 3.851 Å). The observation of ordering peaks confirms the formation of the desired ordered intermetallic phase. The degree of ordering is roughly gauged by comparing the ratio of the (110) and the (111) peaks with the theoretically expected intensity ratio when fully ordered. As shown in Figure S2 (SI), the ratio of the (110) peak to the (111) peak is 0.052, which is close to the values (0.056) in the reference bulk patterns (PDF no. 65-7280), suggesting that Pd_3Fe nanoparticles are almost fully ordered. As shown in Figure 1b,c, for the ordered intermetallic phase of Pd_3Fe, each type of atom (Pd or Fe) occupies its own position, whereas for the disordered alloys of Pd_3Fe, the atomic positions are occupied randomly by Pd and Fe. Annealing conditions have a significant effect on the ordering and particle size of Pd_3Fe. As shown in Figure S3 and Table S1 (SI), an elevated annealing temperature and increasing annealing time favor the formation of the ordered phase, but at the same time annealing promotes the sintering of Pd_3Fe nanoparticles.

An overview TEM image of ordered Pd_3Fe/C and its corresponding particle diameter histograms are presented in Figure 2a and Figure S4a (SI), respectively. As can be seen, Pd_3Fe nanoparticles are highly dispersed on the surface of the

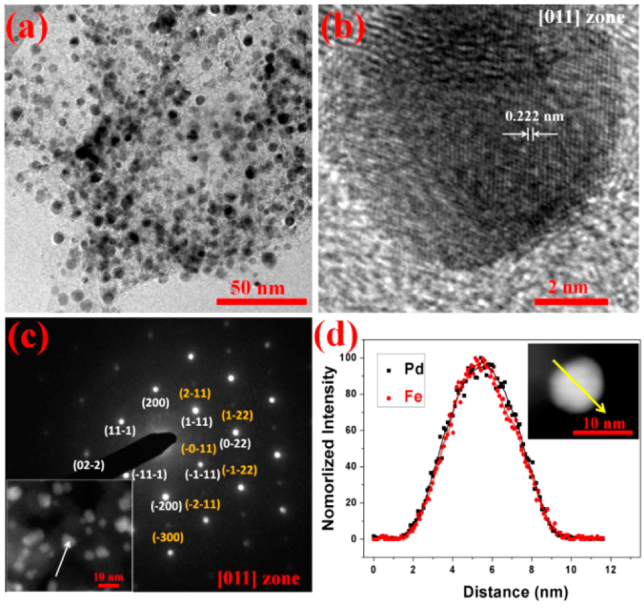

Figure 2. (a) Overview TEM image of ordered Pd_3Fe/C. (b) HR-TEM images of ordered Pd_3Fe/C. (c) D-STEM patterns on the [011] zone axis collected from one particle, shown in the inset. (d) STEM-EDX line scan of Pd_3Fe/C.

carbon support. The histogram of metal nanoparticle diameters is obtained from a sampling size of 100 particles in random regions. It shows a narrow particle size distribution with an average size of 6.1 ± 0.6 nm, which is close to the domain size determined by XRD (5.9 nm). Therefore, the ordered Pd_3Fe nanoparticles are mainly single crystals. The TEM image of disordered Pd_3Fe/C and Pd/C, and the corresponding histograms of their particle sizes, are presented in Figure S4b,c (SI). The average particle sizes for Pd/C and disordered Pd_3Fe/C are 5.8 ± 0.4 and 5.7 ± 0.5 nm, respectively. To visualize better the ordered intermetallic structure, we have also investigated the atomic-level arrangement of Pd and Fe by high-resolution TEM (HR-TEM). Figure 2b shows clear lattice fringes (0.222 nm), corresponding to the (111) plane of cubic Pd_3Fe. Due to the unique superperiod in the ordered phase, ordered arrangements can be directly identified by diffraction patterns. The fast Fourier transforms (FFT) pattern of the Pd_3Fe particle is shown in Figure S5 (SI). The presence of superlattice reflections such as (110) and (210) confirms the ordered structure of Pd_3Fe. Ordered arrangements can be further confirmed by an electron diffraction technique, diffraction STEM (D-STEM), which allows 1−2 nm spatial resolution electron diffraction. Figure 2c shows the clear diffraction patterns on the [011] zone axis collected from the inset particle. Superlattice spacings of 2.722, 1.572, and 1.283 Å are measured for the (110), (210), and (300) superlattice spots in yellow, respectively. The spacing matches with the bulk Pd_3Fe intermetallic structure, and the diffraction pattern aligns with the simulated intermetallic phase (Figure S6, SI). STEM-EDS line spectra of Pd_3Fe/C in Figure 2d suggest that Pd and Fe are uniformly distributed in the nanoparticles.

The atomic ratio of Pd/Fe in Pd_3Fe is analyzed by EDX, which indicates atomic ratios of 3.08 ± 0.2 for ordered Pd_3Fe/C. This result is consistent with the ratios of Pd/Fe in the

DOI: 10.1021/jacs.5b03865
J. Am. Chem. Soc. 2015, 137, 7278−7281

precursors (with Pd/Fe mole ratio of 3). The actual metal loadings in ordered Pd_3Fe/C, disordered Pd_3Fe/C, and Pd/C are 23.4, 24.6, and 20.8 wt %, respectively, which was analyzed by thermogravimetric analysis under air.

The catalytic performance of ordered Pd_3Fe/C for the ORR was evaluated by linear sweep voltammetry (LSV). The polarization curve for a commercial Johnson Matthey Pt/C (20 wt% Pt, ~4.5 nm) catalyst is included for comparison. As shown in Figure 3a, ordered Pd_3Fe/C has an ORR onset

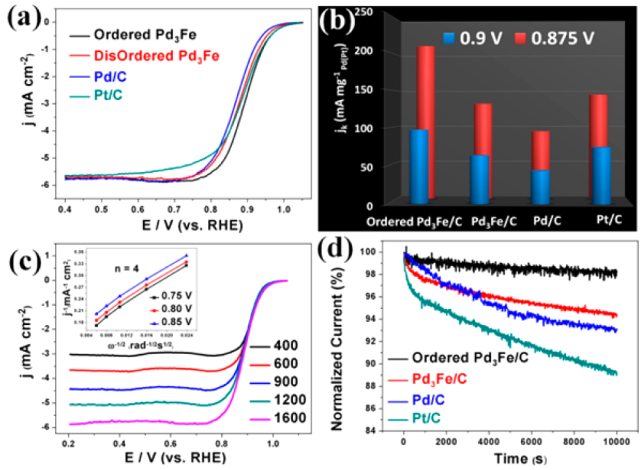

Figure 3. (a) ORR polarization curves in O_2-saturated 0.1 M KOH. Rotation rate, 1600 rpm; sweep rate, 10 mV s^{-1}. (b) Kinetic current (mass activities) at different potentials. (c) Rotation-rate-dependent current–potential curves of ordered Pd_3Fe/C and the corresponding Koutecky–Levich plots at different potentials. (d) Chronoamperometric responses of the samples at 0.8 V in O_2-saturated 0.1 M KOH (percentage of current retained versus operation time).

potential similar to that of Pt/C, which is 30–50 mV higher than those of disordered Pd_3Fe/C and Pd/C. At the beginning of the polarization curves for these catalysts, the current increases exponentially as potential decreases, which is the characteristic of kinetic control. At more negative potentials, the current starts to be controlled mainly by mass transport, until it reaches its diffusion-limited value. In the mixed kinetic/diffusion regime (~0.75 to ~1 V), the electrocatalytic activity of the catalysts can be compared on the basis of the half-wave potentials (the potential at which the current reaches half its diffusion-limited value).[10,14] The half-wave potentials increase in the order of Pd/C < disordered Pd_3Fe/C < Pt/C < ordered Pd_3Fe/C. The ordered Pd_3Fe/C catalyst shows a remarkable positive shift of 10–30 mV relative to the other three catalysts. Such results indicate that ordered Pd_3Fe/C possesses kinetics toward the ORR superior to that of the other three catalysts. The kinetic current (j_k) is calculated using the Koutecky–Levich equation. The mass activities at 0.9 and 0.875 V were calculated from the ORR polarization; the results are shown in Figure 3b. Ordered Pd_3Fe/C exhibits a significantly enhanced mass activity compared to disordered Pd_3Fe/C, Pd/C, and Pt/C. For instance, at 0.9 V, which is the potential usually used for comparing the activities of different catalysts, ordered Pd_3Fe/C produces a current density as high as 97.4 mA mg^{-1}_{Pd}, which is ~1.3–2.2 times higher than those of the other three catalysts. According to previous calculation on Pd-based alloys,[15,16] the enhanced catalytic activity of ordered Pd_3Fe/C may arise from changes in the Pd–Pd bond distance and modification of the electron configuration as well as uniform active sites. The Tafel plots of Pd-based catalysts in Figure S7 (SI) show a low overpotential region above 0.92 V and a high overpotential region below 0.92 V. At the low overpotential region, the slopes of the curves for three Pd-based catalysts are approximately equal. At the high overpotential region, the Tafel slope for ordered Pd_3Fe/C is slightly lower than those for Pd/C and Pd_3Fe/C, suggesting higher activity of the ordered phase. The significant difference in slope between ordered Pd_3Fe/C and Pt/C may be associated with different mechanisms on these two catalysts for the ORR. Figure 3c show the rotation-rate-dependent current–potential curves of ordered Pd_3Fe/C and their corresponding Koutecky–Levich plots at different potentials. Similar curves for disordered Pd_3Fe/C and Pd/C are given in Figure S8 (SI). Based on the slopes of the Koutecky–Levich plots, the electron transfer numbers (n) are calculated to be ~4 for ordered Pd_3Fe/C at 0.75–0.85 V, indicating the nearly complete reduction of O_2 to H_2O on the surface of the ordered Pd_3Fe catalyst. The durability of the catalysts was assessed by chronoamperometry at a fixed potential of 0.8 V (vs RHE). Measurements were performed in O_2-saturated 0.1 M KOH with a rotation rate of 1600 rpm. As shown in Figure 3d, continuous oxygen reduction on ordered Pd_3Fe/C causes only a 2% degradation in current density. In contrast, a larger activity loss is observed in the other three catalysts: ~6% for disordered Pd_3Fe/C, ~7% for Pd/C, and ~11% for Pt/C. The higher stability of the ordered Pd_3Fe phase is mainly due to the high enthalpy of mixing. In addition, as shown in Figure 1b, in an ordered phase the Fe atoms are surrounded by 12 nearest-neighbor Pd atoms, resulting in the blocking of Fe-leaching channels. In the disordered Pd_3Fe phase, as shown in Figure 1c and Figure S9 (SI), some Fe atoms are near neighbors; if one of them is leached out, the near-neighbor Fe atoms will be more likely to be leached out as well. Regarding the stability of Pt/C, it is well known that Pt nanoparticles suffer from dissolution and migration problems.[17]

The catalytic performances of ordered Pd_3Fe/C and conventional Pt/C are also compared in a rechargeable hybrid Li–air battery with $NiCo_2O_4$ grown onto a Ni foam (NCONF@Ni),[2] serving as the catalyst for the oxygen evolution reaction. The XRD pattern and SEM image of NCONF@Ni are presented in Figure S10 (SI). Figure 4a shows the polarization curve of hybrid Li–air cells obtained by LSV at 5 mV s^{-1}. The curve for ordered Pd_3Fe/C almost overlaps that for Pt/C, indicating that these two catalysts have similar activities for the ORR in hybrid Li–air cells. For both curves, the abrupt drop at the beginning is due to the activation polarization, and the remaining curves, which are almost linear, are due to the large resistance of the solid electrolyte.[2,18] The maximum power densities are calculated to be 11.7 mW cm^{-2} for ordered Pd_3Fe/C and 12.3 mW cm^{-2} for Pt/C. Figure 4b,c shows the cycling performance of hybrid Li–air batteries with ordered Pd_3Fe/C and Pt/C as ORR catalysts. Their discharge and charge voltage profiles are split into two branches because the discharge and charge data were collected by two independent channels alternately with an Arbin battery tester. For the battery with ordered Pd_3Fe/C as the ORR catalyst, the round-trip overpotential increases from 0.9 V at the first cycle to 0.92 V at the 55th cycle and to 0.98 V at the 220th cycle. In the case of the cell with Pt/C as ORR catalyst, the round-trip overpotential is 0.9 V initially, and it increases to 1.31 V at the 55th cycle, which is similar to the reported results.[19] After 55 cycles, the battery with ordered Pd_3Fe/C only increases by 2.2% relative to the initial round-trip overpotential, which is

DOI: 10.1021/jacs.5b03865
J. Am. Chem. Soc. 2015, 137, 7278–7281

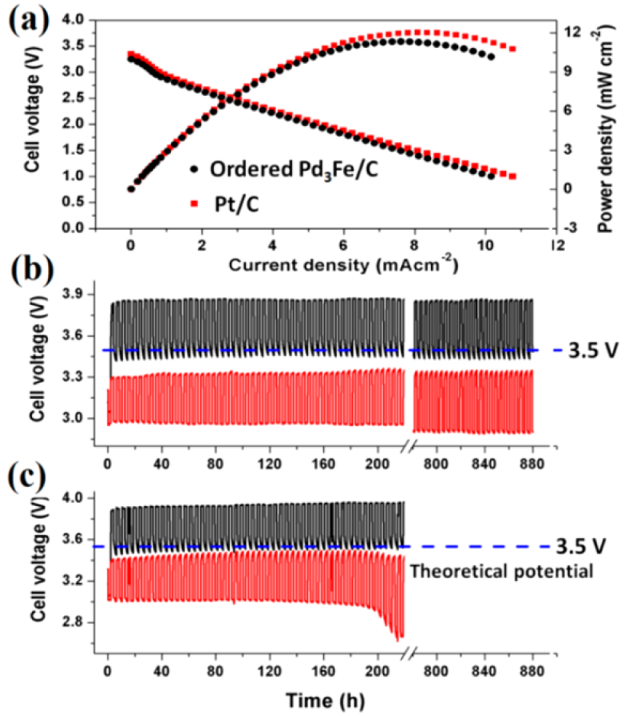

Figure 4. (a) ORR polarization curves of ordered Pd_3Fe/C and Pt/C catalysts in hybrid Li–air cells. Cycling performance of the hybrid Li–air batteries with (b) ordered Pd_3Fe/C + NCONF@Ni air electrode and (c) the conventional Pt/C + NCONF@Ni air electrode.

much lower than that for the battery with Pt/C (45.5%), indicating that the ordered Pd_3Fe/C catalyst significantly enhances the cycling stability of hybrid Li–air batteries. Furthermore, for the cell with ordered Pd_3Fe/C, long-term charge–discharge for 880 h (220 cycles) results in only a 0.08 V increase in round-trip overpotential, which is the best cycling performance reported so far (Table S2, SI).[2,19−24] Since all tests are performed under the same conditions, the difference in cycling performances of these two cells is mainly associated with the difference of the intrinsic stability of the two ORR catalysts.

In conclusion, a structurally ordered Pd_3Fe intermetallic compound with small particle size was successfully synthesized in THF solvent with KEt_3BH as reducing agent. KCl is an insoluble byproduct of the reaction and serves as a matrix that traps the nanoparticles, preventing particle agglomeration. For the ORR in alkaline media, ordered Pd_3Fe/C catalysts exhibit much higher activity and durability than disordered Pd_3Fe/C, Pd/C, and Pt/C. The ordered Pd_3Fe/C catalyst enables long-term cycling performance of hybrid Li–air batteries over 880 h with only a 0.08 V increase in round-trip overpotential. The extraordinarily high performance of ordered Pd_3Fe/C catalyst provides a very promising alternative to the conventional Pt/C catalyst for an air cathode in alkaline electrolyte.

■ ASSOCIATED CONTENT

Supporting Information

Synthesis of Pd_3Fe/C and Pd/C; electrode preparation and electrochemical measurements; XRD patterns and TEM images.The Supporting Information is available free of charge on the ACS Publications website at DOI: 10.1021/jacs.5b03865.

■ AUTHOR INFORMATION

Corresponding Author

*jgoodenough@mail.utexas.edu

Author Contributions

#Z.C. and L.L. contributed equally.

Notes

The authors declare no competing financial interest.

■ ACKNOWLEDGMENTS

This work was supported by the U.S. Department of Energy, Office of Basic Energy Sciences, Division of Materials Science and Engineering under award number DE-SC0005395. We thank Dr. Karalee Jarvis for assistance with TEM data acquisition and analysis. J.B.G. acknowledges the support from the Robert A. Welch Foundation (Grant F-1066).

■ REFERENCES

(1) Lu, J.; Li, L.; Park, J.-B.; Sun, Y.-K.; Wu, F.; Amine, K. *Chem. Rev.* **2014**, *114*, 5611.
(2) Li, L.; Chai, S.-H.; Dai, S.; Manthiram, A. *Energy Environ. Sci.* **2014**, *7*, 2630.
(3) Jiao, Y.; Zheng, Y.; Jaroniec, M.; Qiao, S. Z. *Chem. Soc. Rev.* **2015**, *44*, 2060.
(4) Yang, W.; Fellinger, T. P.; Antonietti, M. *J. Am. Chem. Soc.* **2011**, *133*, 206.
(5) Zhou, R.; Qiao, S. Z. *Chem. Commun.* **2015**, *51*, 7516.
(6) Liang, Y. Y.; Li, Y. G.; Wang, H. L.; Zhou, J. G.; Wang, J.; Regier, T.; Dai, H. J. *Nat. Mater.* **2011**, *10*, 780.
(7) Wu, Z. S.; Yang, S. B.; Sun, Y.; Parvez, K.; Feng, X. L.; Mullen, K. *J. Am. Chem. Soc.* **2012**, *134*, 9082.
(8) Cheng, F. Y.; Shen, J. A.; Peng, B.; Pan, Y. D.; Tao, Z. L.; Chen, J. *Nat. Chem.* **2011**, *3*, 79.
(9) Maheswari, S.; Karthikeyan, S.; Murugan, P.; Sridhar, P.; Pitchumani, S. *Phys. Chem. Chem. Phys.* **2012**, *14*, 9683.
(10) Lu, Y.; Jiang, Y.; Gao, X.; Wang, X.; Chen, W. *J. Am. Chem. Soc.* **2014**, *136*, 11687.
(11) Cui, Z. M.; Chen, H.; Zhao, M. T.; Marshall, D.; Yu, Y. C.; Abruna, H.; DiSalvo, F. J. *J. Am. Chem. Soc.* **2014**, *136*, 10206.
(12) Wang, D. L.; Xin, H. L. L.; Hovden, R.; Wang, H. S.; Yu, Y. C.; Muller, D. A.; DiSalvo, F. J.; Abruna, H. D. *Nat. Mater.* **2013**, *12*, 81.
(13) Chen, H.; Wang, D.; Yu, Y.; Newton, K. A.; Muller, D. A.; Abruña, H.; DiSalvo, F. J. *J. Am. Chem. Soc.* **2012**, *134*, 18453.
(14) Garsany, Y.; Baturina, O. A.; Swider-Lyons, K. E.; Kocha, S. S. *Anal. Chem.* **2010**, *82*, 6321.
(15) Shao, M.; Liu, P.; Zhang, J.; Adzic, R. *J. Phys. Chem. B* **2007**, *111*, 6772.
(16) Fernández, J. L.; Walsh, D. A.; Bard, A. J. *J. Am. Chem. Soc.* **2005**, *127*, 357.
(17) Wang, Y. J.; Wilkinson, D. P.; Zhang, J. J. *Chem. Rev.* **2011**, *111*, 7625.
(18) Li, L.; Manthiram, A. *Nano Energy* **2014**, *9*, 94.
(19) Yoo, E.; Zhou, H. *ACS Nano* **2011**, *5*, 3020.
(20) Yang, W.; Salim, J.; Li, S.; Sun, C.; Chen, L.; Goodenough, J. B.; Kim, Y. *J. Mater. Chem.* **2012**, *22*, 18902.
(21) Li, Y.; Huang, Z.; Huang, K.; Carnahan, D.; Xing, Y. *Energy Environ. Sci.* **2013**, *6*, 3339.
(22) Stevens, P.; Toussaint, G.; Caillon, G.; Viaud, P.; Vinatier, P.; Cantau, C.; Fichet, O.; Sarrazin, C.; Mallouki, M. *ECS Trans.* **2010**, *28*, 1.
(23) Zhou, H.; Wang, Y.; Li, H.; He, P. *ChemSusChem* **2010**, *3*, 1009.
(24) Zhang, T.; Imanishi, N.; Shimonishi, Y.; Hirano, A.; Takeda, Y.; Yamamoto, O.; Sammes, N. *Chem. Commun.* **2010**, *46*, 1661.

DOI: 10.1021/jacs.5b03865
J. Am. Chem. Soc. 2015, 137, 7278−7281